ISBN: 978-3-95450-230-1 ISSN: 2673-5350 doi:10.18429/JACoW-IBIC2021-WEOA04

BUNCH-RESOLVED 2D DIAGNOSTICS – STREAKING COMBINED WITH INTERFEROMETRY*

M. Koopmans†[1], J.-G. Hwang, A. Jankowiak[1], M. Ries, G. Schiwietz
Helmholtz-Zentrum Berlin für Materialien und Energie GmbH (HZB), Berlin, Germany
[1]also at Humboldt-Universität zu Berlin, Berlin, Germany

Abstract

Due to the complexity of the fill pattern in the BESSY II electron-storage ring, bunch-resolved diagnostics are required for machine commissioning and to ensure the long-term quality and stability of operation. In addition, low-α operation and a possible VSR upgrade demand bunch-length measurements with picosecond resolution. Therefore, a dedicated beamline equipped with a fast streak camera was set up and successfully commissioned. Couplings between time- and space-coordinates also call for bunch-selective and correlated multi-parameter detection methods. Thus, the beamline and the streak camera have been made capable of direct beam-profile imaging and interferometry of the vertical beam size using the X-ray blocking baffle method. The horizontal or vertical dimension can additionally be imaged with the streak camera and bunch-resolved 2D measurements are possible. Imaging the vertical direction, the characteristic dip in the center of the interference pattern from the π-polarized synchrotron radiation can be observed and is used to extract bunch resolved information about the vertical beam size. The streak camera measurements are validated with direct imaging measurements with a regular CCD camera at the beamline and compared to model calculations. The results are converted into absolute values by a calibration with the BESSY II pinhole monitors.

INTRODUCTION

The BESSY II electron storage ring provides synchrotron radiation (SR) to a very diverse user community. In standard user operation a complex fill pattern features multiple bunch types for dedicated applications. Special operation modes like single bunch or low-α operation for short pulses are offered for few weeks a year [1, 2]. In addition, a new operation with a second orbit is tested and developed [3] and a possible upgrade to a variable pulse length storage ring (VSR) is envisioned [1].

Non-invasive bunch resolved diagnostics are needed for maintaining and improving of existing as well as for commissioning and development of new operation modes. For this purpose dedicated diagnostic beamlines have been installed. A new beamline dedicated for bunch resolved longitudinal diagnostics equipped with a fast streak camera has been commissioned and is in full operation since mid 2020 [4]. Although this beamline is optimized for maximum photon flux, it has extremely good transverse imaging capabilities. Furthermore, the streak camera features an entrance aperture with a horizontal slit. Depending on the beamline settings, it is possible to image either a slice corresponding to the horizontal or the vertical direction of the initial electron beam in the horizontal direction of the streak camera. In combination with the streak camera an RMS resolution down to 120 µm was reached for direct imaging in the transverse direction. It was also shown that bunch position fluctuations below 10 µm (RMS) can be measured applying a statistical analysis method to single shot streak camera images [5].

To overcome the resolution limit of direct imaging, a combination of interferometry with the streak camera is investigated to become sensitive to bunch sizes below 120 µm [6]. For this goal the interference in the vertical direction originating from the X-ray blocking baffle using π-polarized SR turned out to be very promising. This method is similar to the obstacle diffractometer method introduced in Ref. [7, 8].

VERTICAL BEAMLINE IMAGING

A simplified schematic of the longitudinal diagnostics beamline at BESSY II, which contains the components relevant for the vertical imaging, is shown in Fig. 1. The SR beam first passes the X-ray blocking baffle and is then collimated through an intermediate focus with the M1 ellipsoid and the M2 toroid mirrors, which are replaced by lenses in the schematic. Then a polarisation filter, followed by a 90° rotation of the SR beam with a periscope (not shown in Fig. 1) and a 700 nm bandpass filter (10 nm FWHM bandwidth) are used to obtain a clear interference pattern, which is finally detected with a regular CCD or the streak camera. Additionally, a slit with an opening aperture of 2 mm is used to cut out approximately an eighth of the collimated beam for improved coherence due to the varying quality along the beam profile. The region with a minimal wavefront error was chosen by adjusting the slit position to optimize the

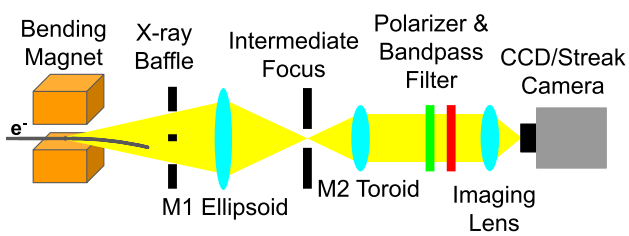

Figure 1: Schematic of the relevant objects for vertical imaging at the longitudinal diagnostics beamline at BESSY II. The two mirrors are replaced by lenses in this linearized drawing by keeping the main optical properties (M1 for point-to-point focussing and M2 for collimation).

* Work supported by the German Bundesministerium für Bildung und Forschung, Land Berlin and grants of the Helmholtz Association
† marten.koopmans@helmholtz-berlin.de

ISBN: 978-3-95450-230-1 ISSN: 2673-5350 doi:10.18429/JACoW-IBIC2021-WEOA04

interference pattern at the CCD camera.

An example image of the interference pattern for π-polarized SR, measured with the CCD camera at the focus of a 75 cm focal length achromat lens, can be found in Fig. 2. Note that all data presented in this paper are taken with the rotated beamline configuration. This enables measuring the vertical interference pattern also in the horizontal direction of the streak camera. Therefore, the directions corresponding to the electron beam are switched in the CCD camera image. Two separate peaks for π-polarized SR are observed due to a destructive interference in the center. The interference fringes extend to large distances and are still visible 250 Pixel away from the center. Within this paper only the projection corresponding to the vertical beam direction (imaged in horizontal CCD or streak camera direction) will be analyzed and discussed.

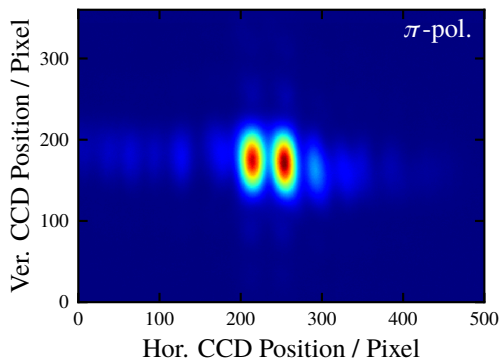

Figure 2: CCD camera interference image taken with π-polarized SR using a 700 nm bandpass filter. The horizontal axis in the image corresponds to the initial vertical beam direction and vice-versa.

MEASUREMENTS WITH VARIABLE VERTICAL BEAM SIZE

A measurement series with variable beam size was conducted to further verify the method and show that it is in principle possible to obtain high resolution bunch-resolved quantitative results for the vertical bunch size with the streak camera. For this purpose the BESSY II feature for a blow-up of the vertical beam size by a white noise excitation is used, with which the vertical beam size can be increased by up to a factor of 6 at maximum excitation. Variation of the vertical beam size by this excitation is a very useful tool for lifetime studies or to obtain resolution limits in combination with beam loss monitor measurements as presented in Refs. [6, 9]. Here the excitation is also used to vary the vertical beam size, while observing the interference pattern with the CCD and the streak camera. Finally the properties of the measured interference patterns are correlated with the beam size at the source point of the beamline and accurate quantitative results can be given.

CCD Camera Measurements

First the interference patterns obtained from bunch averaged measurements with the regular CCD camera are presented. The measurements were performed in the same setup as described above. The obtained projections of the interference patterns corresponding to the vertical beam size at different white noise excitation amplitudes applied to the beam are shown for both polarisations in Fig. 3.

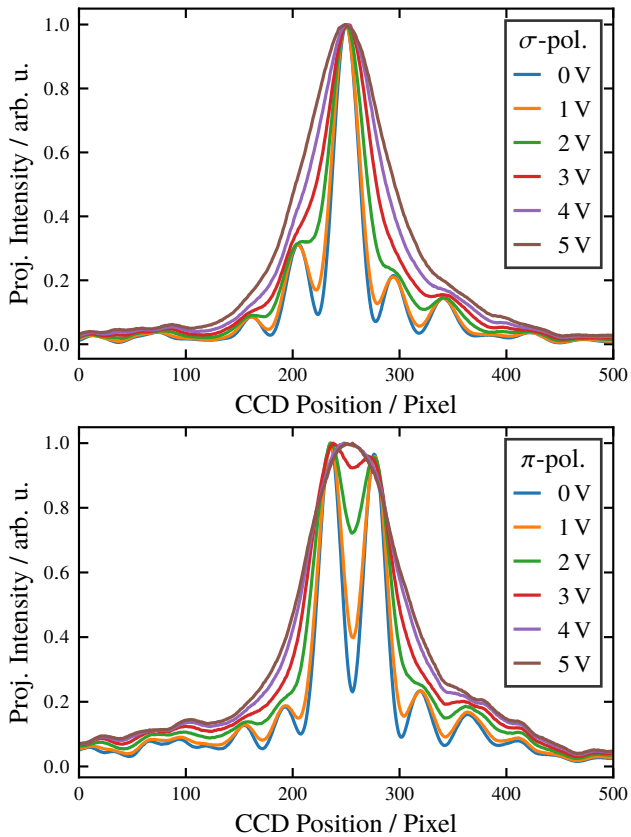

Figure 3: Projections of the interference pattern corresponding to the vertical beam direction for σ (top) and π-polarized SR (bottom) from measured CCD camera images at a wavelength of 700 nm for different white noise excitation settings to manipulate the vertical beam size.

The averaged distance between the different interference maxima at the CCD camera is about 41 pixels (with a pixel size of 4.54 µm). This includes both polarisations settings and also the distance between the two main peaks for π-polarized SR. The effect of changing the beam size can be nicely observed in the projection of the interference pattern. For increasing beam sizes the visibility decreases and the interference pattern is smoothed out for both polarisations until only the envelope remains at high excitations. For the interference pattern of σ-polarized SR this results mainly in a broadening of the central peak. For π-polarized SR the central dip in the interference pattern is visible, but vanishes when beam excitations corresponding to a set value above 3 volt are applied.

ISBN: 978-3-95450-230-1 ISSN: 2673-5350 doi:10.18429/JACoW-IBIC2021-WEOA04

Streak Camera Measurements

It was now attempted to image the vertical interference in the horizontal direction of the streak camera. Measurement images taken during the manipulation of the vertical beam size with the white excitation are shown without and with maximum excitation for π-polarized SR in Fig. 4. The fill pattern was modified to include a separated bunch with the same current as the train bunches (slightly below 1 mA).

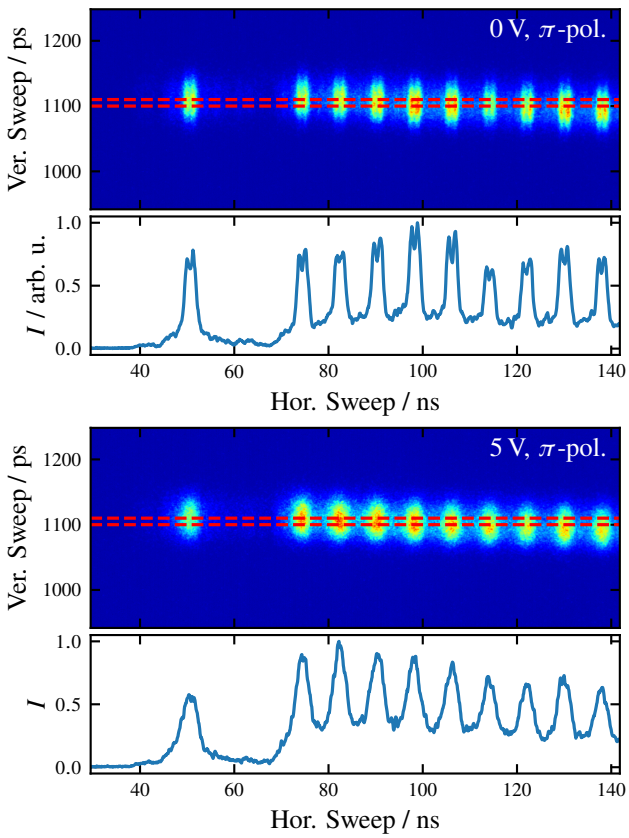

Figure 4: Streak camera images taken with π-polarized SR using a 700 nm bandpass filter imaging the vertical interference in the horizontal direction streak camera direction for minimal vertical bunch sizes (top, 0 V excitation) and maximal vertical bunch sizes (bottom, 5 V excitation).

In the vertical direction a fast sweep is applied and the bunch length can be obtained from this direction in the streak camera image. In the horizontal direction a slow sweep is used to separate the bunch spots corresponding to the fill pattern in the horizontal direction in the streak camera image. In addition, for each single bunch the interference pattern similar as measured with the CCD camera can be recognized. Due to the smaller magnification and the conversion processes in the streak camera, the resolution of the streak camera is worsened compared to the CCD camera. It is also clearly visible that the interference patterns smooth out, the intensity spots get broader and the central dips in the interference patterns vanish with increasing excitation. Note that due to the limited intensity from collimation and the used filters quite long integration times are required. For the displayed streak camera images analog integrations of 1000 continuous acquisitions with exposure times of 120 ms were used.

For comparison of the properties of the projected interference patterns measured with the CCD camera, an average train bunch projection is calculated from all train bunches detected in the streak camera images. The average train bunch projections from the streak camera measurements are shown for different excitation settings and for both polarisations in Fig. 5.

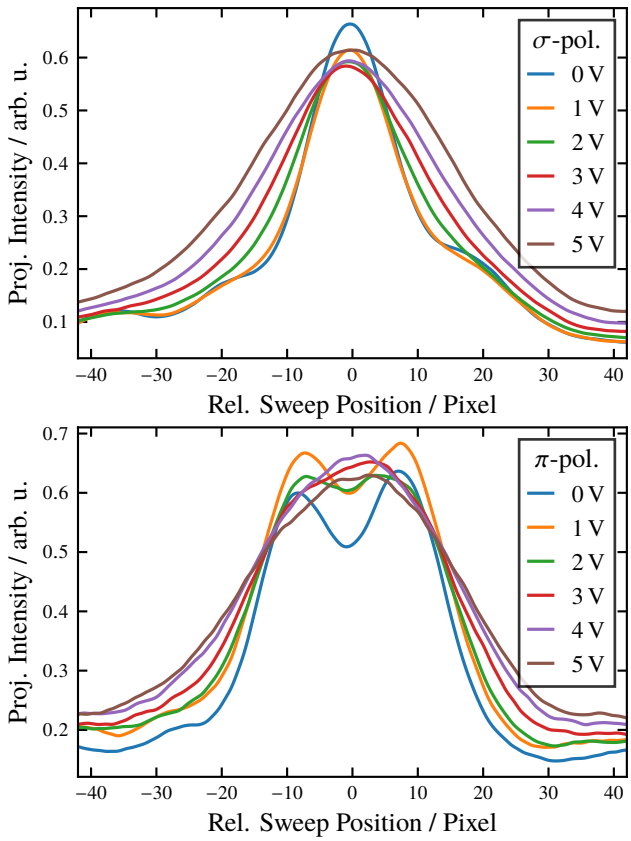

Figure 5: Average train bunch projections of the interference pattern corresponding to the vertical beam direction for σ (top) and π-polarized SR (bottom) from measured streak camera images at a wavelength of 700 nm for different white noise excitation settings to manipulate the vertical beam size.

One can recognize the slight broadening of the central peaks for both polarisations and the central dip of the π-polarized SR disappears for larger vertical beam sizes with increasing excitation. In comparison to the CCD camera measurements the central dip of the interference pattern for π-polarized SR is only visible for an excitation setting up to about 2 V. Note that the intensity between the train bunches in the streak images does not drop to 0 and the effect of overlapping interference patterns in the streak camera (Fig. 4) increases for larger beam sizes.

ISBN: 978-3-95450-230-1 ISSN: 2673-5350 doi:10.18429/JACoW-IBIC2021-WEOA04

Quantitative Results

For direct comparison of the CCD and the streak camera measurements, the respective pixel values of both systems are converted into absolute source-point positions using the known image magnifications. As a reference value the pinhole monitors [10] for transverse beam size measurements were used and a calibration as presented in Ref. [6] was performed. Using the measured resolution of the pinhole systems the true beam sizes at the respective source points are estimated as function of the excitation set value. The expected beam size at the source point of longitudinal diagnostics beamline is then calculated via the vertical β-functions from the standard BESSY II lattice model.

The FWHM widths of the central peak or the two central peaks depending on the selected polarisation in the interference pattern measured at the CCD and the streak camera are shown as a function of the estimated FWHM beam size in Fig. 6. The measured FWHM widths in the interference

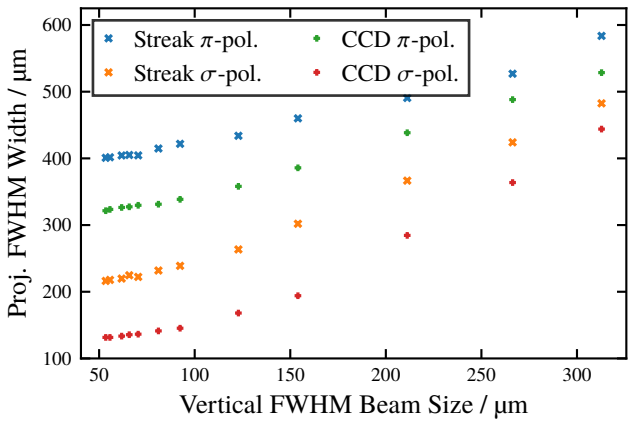

Figure 6: FWHM widths obtained from the central interference maxima for σ and π-polarized SR of the projections from CCD camera images and average train bunch projections of streak camera measurements converted to dimensions corresponding to the source points as a function of the estimated vertical FWHM bunch size.

patterns for both polarisations and both devices increase monotonously. With the CCD camera a FWHM width of the central peak down to about 120 µm (50 µm RMS) and for the streak camera an improved FWHM resolution below 220 µm (93 µm RMS) is reached. The details functional dependencies can be understood considering the ideal interference patterns, the true beam size and the resolution of the systems.

Even more interesting is the central dip for π-polarized SR. The peak-dip ratio R is calculated as the ratio of the intensity at the central dip divided by the averaged intensity at the two surrounding peaks. The obtained peak-dip ratios from the CCD and streak camera measurements are shown as a function of the vertical beam size in Fig. 7.

The peak-dip ratios obtained from the CCD camera images range between about 0.23 for the minimum beam size and 1 (no dip) for vertical beam sizes above 100 µm. The

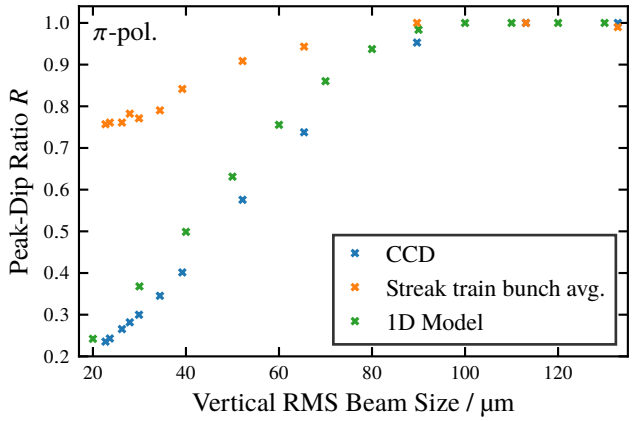

Figure 7: Peak-dip ratio as a function of the vertical RMS beam size obtained from the central minima of the interference patterns of π-polarized SR from measurements of CCD and streak camera projections for the average train bunch, and from 1D model calculations.

variation of R is significantly reduced for the streak camera. Here the minimum measured peak-dip ratio is about 0.75 and a value of 1 is reached already below a vertical RMS beam size of 90 µm. Nevertheless, a region were the peak-dip ratio has a clear dependency on the vertical beam size is observed and the RMS resolution is estimated to be about 10 µm. The results are again consistent considering the resolution of the streak camera and the image magnifications of both systems. In addition the peak dip ratios obtained from CCD camera measurements are compared with 1D model calculations. The general behavior is similar, but the deviations are not negligible. Investigation are ongoing, so that the model can also be used as a reference to obtain the beam size from measurements of R.

CONCLUSION

Together with the standard longitudinal bunch length measurements, it is possible to image interference patterns with a streak camera corresponding to the vertical beam direction at our beamline. Vertical bunch sizes below 90 µm (RMS) can be resolved with the method and quantitative results with an accuracy of about 10 µm (RMS) can be obtained using a calibration. Further improvements for higher resolution are tested. The outer interference fringes can be blocked with the slit at the intermediate focus. Therefore, the spots of individual bunches are well separated at the streak camera and the focal length of the final lens may be increased to enlarge the interference patterns.

REFERENCES

[1] A. Jankowiak *et al.*, Eds., "BESSY VSR – Technical Design Study", Helmholtz-Zentrum Berlin für Materialien und Energie GmbH, Germany, 2015. doi:10.5442/R0001

[2] R. Müller *et al.*, "BESSY II Supports an Extensive Suite of Timing Experiments", in *Proc. 7th Int. Particle Accelerator*

ISBN: 978-3-95450-230-1 ISSN: 2673-5350 doi:10.18429/JACoW-IBIC2021-WEOA04

Conf. (IPAC'16), Busan, Korea, May 2016, pp. 2840–2843. doi:10.18429/JACoW-IPAC2016-WEPOW011

[3] P. Goslawski *et al.*, "Two Orbit Operation at Bessy II - During a User Test Week", in *Proc. 10th Int. Particle Accelerator Conf. (IPAC'19)*, Melbourne, Australia, May 2019, pp. 3419–3422. doi:10.18429/JACoW-IPAC2019-THYYPLM2

[4] G. Schiwietz *et al*., "Bunch-resolved diagnostics for a future electron-storage ring", *Nuclear Instruments and Methods in Physics Research Section A: Accelerators, Spectrometers, Detectors and Associated Equipment*, vol. 990, p. 164992, 2021. doi:10.1016/j.nima.2020.164992

[5] M. Koopmans *et al.*, "Statistical Analysis of 2D Single-Shot PPRE Bunch Measurements", presented at the 12th Int. Particle Accelerator Conf. (IPAC'21), Campinas, Brazil, May 2021, paper MOPAB296.

[6] M. Koopmans *et al.*, "Vertical Beam Size Measurement Methods at the BESSY II Storage Ring and their Resolution Limits", in *Proc. 10th Int. Particle Accelerator Conf. (IPAC'19)*, Melbourne, Australia, May 2019, pp. 2491–2494. doi:10.18429/JACoW-IPAC2019-WEPGW012

[7] J. Breunlin et al., "Methods for measuring sub-pmrad vertical emittance at the Swiss Light Source", *Nuclear Instruments and Methods in Physics Research Section A: Accelerators, Spectrometers, Detectors and Associated Equipment*, vol. 803, pp. 55–64, 2015. doi:10.1016/j.nima.2015.09.032

[8] Å. Anderson *et al.*, "Diagnostics at the Max IV 3 GeV Storage Ring During Commissioning", in *Proc. 5th Int. Beam Instrumentation Conf. (IBIC'16)*, Barcelona, Spain, Sep. 2016, pp. 1–5. doi:10.18429/JACoW-IBIC2016-MOAL02

[9] M. Koopmans, "Interferometric Beam Size Monitor for BESSY II", Master thesis, Humboldt-Universität zu Berlin, Berlin, Germany, 2017.

[10] K. Holldack, J. Feikes and W. B. Peatman, "Source size and emittance monitoring on BESSY II", *Nuclear Instruments and Methods in Physics Research Section A: Accelerators, Spectrometers, Detectors and Associated Equipment*, vol. 467, pp. 235–238, 2001.